Bioactive Materials 28 (2023) 348–357

Contents lists available at ScienceDirect

Bioactive Materials

journal homepage: www.keaipublishing.com/en/journals/bioactive-materials

Design and fabrication of high-performance injectable self-setting trimagnesium phosphate

Jiawei Liu [a,1], Wen Hou [a,1], Wenying Wei [a], Jian Peng [a], Xiaopei Wu [a], Chenxi Lian [a], Yanan Zhao [a], Rong Tu [b], Takashi Goto [c], Honglian Dai [a,b,*]

[a] State Key Laboratory of Advanced Technology for Materials Synthesis and Processing, Biomedical Materials and Engineering Research Center of Hubei Province, Wuhan University of Technology, Wuhan 430070, China
[b] Chaozhou Branch of Chemistry and Chemical Engineering Guangdong Laboratory, Chaozhou 521000, China
[c] New Industry Creation Hatchery Center, Tohoku University, Sendai 980-8579, Japan

ARTICLE INFO

Keywords:
Bone cement
Trimagnesium phosphate
High compressive strength
Injectable
Bioactive materials

ABSTRACT

Magnesium phosphate bone cement has become a widely used orthopedic implant due to the advantages of fast-setting and high early strength. However, developing magnesium phosphate cement possessing applicable injectability, high strength, and biocompatibility simultaneously remains a significant challenge. Herein, we propose a strategy to develop high-performance bone cement and establish a trimagnesium phosphate cement (TMPC) system. The TMPC exhibits high early strength, low curing temperature, neutral pH, and excellent injectability, overcoming the critical limitations of recently studied magnesium phosphate cement. By monitoring the hydration pH value and electroconductivity, we demonstrate that the magnesium-to-phosphate ratio could manipulate the components of hydration products and their transformation by adjusting the pH of the system, which will influence the hydration speed. Further, the ratio could regulate the hydration network and the properties of TMPC. Moreover, in vitro studies show that TMPC has outstanding biocompatibility and bone-filling capacity. The facile preparation properties and these advantages of TMPC render it a potential clinical alternative to polymethylmethacrylate and calcium phosphate bone cement. This study will contribute to the rational design of high-performance bone cement.

Credit authorship contribution statement

Jiawei Liu: Investigation, Formal analysis, Writing – original draft, Methodology. Wen Hou: Validation, Investigation, Methodology. Wenying Wei: Visualization, Validation, Writing – review & editing. Jian Peng: Writing – review & editing. Xiaopei Wu: Writing – review & editing. Chenxi Lian: Investigation. Yanan Zhao: Review. Rong Tu: Supervision, Writing – review & editing. Takashi Goto: Writing – review & editing. Honglian Dai: Supervision, Writing – review & editing, Funding acquisition, Conceptualization, Project administration.

1. Introduction

Due to its self-curing characteristics, bone cement has become a promising orthopedic implant to fill irregular defects or as a drug carrier to treat bone defects [1–3]. To our knowledge, bone cement should be biocompatible, biodegradable, and equipped with several features, such as outstanding injectability to fill defects, anti-washout properties to avoid leakage, and low curing temperature to minimize tissue damage [4]. Furthermore, rapid strength development and high mechanical strength are also necessary. Polymethyl methacrylate (PMMA), which has high mechanical strength and rapid strength development properties, has been the most commonly used bone cement in clinic for decades. However, the exothermic polymerization and cement leakage hinder its wide applications [5–7]. Meanwhile, the non-degradability and lack of biological activity make it difficult for PMMA to promote bone integration and healing. Thus, degradable inorganic bone cement has been developed, especially the bone-like phosphate cement such as

Peer review under responsibility of KeAi Communications Co., Ltd.
* Corresponding author. State Key Laboratory of Advanced Technology for Materials Synthesis and Processing, Biomedical Materials and Engineering Research Center of Hubei Province, Wuhan University of Technology, Wuhan 430070, China.
E-mail address: daihonglian@whut.edu.cn (H. Dai).
[1] Equal contribution.

https://doi.org/10.1016/j.bioactmat.2023.05.019
Received 7 January 2023; Received in revised form 29 May 2023; Accepted 30 May 2023

calcium phosphate cement (CPC) and magnesium phosphate cement (MPC). Although CPC with osteoinductivity and biodegradability has been applied as a substitute for PMMA for young patients in particular [8], it is limited by its poor mechanical behavior and injectability [9,10].

First used in dentistry, MPC, traditionally based on magnesium oxide and potassium dihydrogen phosphate, has attracted much attention in orthopedic implants. As a kind of fast-setting cement, it possesses several advantages, such as high early strength, rapid strength development, and low shrinkage [11]. Notably, magnesium is one of the significant elements in the human body and is predominantly stored in bone tissue [12]. Moreover, magnesium has been reported to have multiple biological effects that contribute to bone and vascularization [13–16]. The widely studied MPCs are based on the dissolution-precipitation reaction, which forms a continuous matrix of binder phase K-struvite ($MgKPO_4{\cdot}6H_2O$). This binder phase possesses good mechanical and biodegradable properties and is the main curing product of MPCs [17]. However, the hydration of MPC generates heat and alkalinity from the dissolution of MgO, which accelerates the formation of K-struvite and impairs the injectability and operability in clinic [18]. In addition, the newly formed K-struvite on the surface of MgO during crystallization will inhibit further hydration. Thus, controlling the formation rate of K-struvite is the key to controlling MPC performance. In industrial applications, using excessive MgO is the general way to ensure an adequate K-struvite formation rate and achieve high strength [18,19]. But the induced alkaline environment (usually pH 9–10) may hinder tissue regeneration [20,21]. Researchers have tried to address these problems by incorporating retarders [11,18], polymers [22–24], and other inorganic salts [25]. However, introducing more components will adversely affect the mechanical strength of MPC cement and make the system too complex for clinical translation. Consequently, developing bioactive bone cement with applicable injectability and high strength remains challenging.

Therefore, our design aims to find a simple method to solve these shortcomings. To this end, we used a bio-ceramic trimagnesium phosphate ($Mg_3(PO_4)_2$, TMP) to replace MgO and successfully developed a trimagnesium phosphate-potassium dihydrogen phosphate (KDP)-H_2O (TMP-KDP-H_2O) ternary cement system (TMPC). In this system, TMP acted as a magnesium source and the dissolution of TMP provided the driving force for hydration. Distinguished from MgO, $Mg_3(PO_4)_2$, a biocompatible ceramic, could provide an alkalescent environment and the phosphate ions to ensure an adequate reaction. TMPC has the advantages of high strength, low curing temperature, neutral pH environment, and reliable injectability. Further, we conducted a comprehensive study on setting time, injectability, compressive strength, hydration product, and morphology of TMPC with different magnesium-to-phosphate (M/P) ratios. We also studied the hydration mechanism of TMPC and found that the M/P ratio could manipulate the hydration process. Overall, this study provides a high-performance MPC bone cement for clinical use and offers a theoretical basis for its design.

2. Experimental section

2.1. Raw powder preparation and characterization

TMP powder was synthesized by solid-state reaction and ball milling. Briefly, 144 g $MgHPO_4{\cdot}3H_2O$ (AR, Macklin, China) and 24 g $Mg(OH)_2$ (AR, Macklin, China) were mixed by a planetary ball mill (BM6Pro, POWTEQ) for 2 h at 250 rpm. Then it was sintered at 1150 °C for 5 h. The obtained sintered cake was crushed by ball milling for 18 h at 300 rpm. KH_2PO_4 (AR, Sinopharm, China) was crushed by ball milling for 6 h at 300 rpm. X-ray diffraction (XRD, Empyrean, Netherlands) was used to analyze the phase and purity of TMP and KDP with Cu (Kα). Diffraction data were collected in the 2θ range from 10° to 60°, with an increment of 0.03° and 0.3 s per step. Particle size distribution and Brunauer–Emmett–Teller (BET) surface of powder were characterized by laser particle analyzer (Bettersize 2600, China) and surface area and pore size analyzer (TriStarII 3020, Micromeritics, USA). The element purity was analyzed by inductively coupled plasma optical emission spectroscopy (ICP-OES, Prodigy 7, ICP-OES - Teledyne Leeman Labs, USA).

2.2. Preparation and characterization of TMPC

TMP and KDP powder were dry mixed in a disperser (ULTRA-TURRAX, IKA, Germany) with a ball milling tube at different M/P ratios (weight ratio) for 1 min. The ratios studied in this study are shown in Table S2. The powders and liquids at different powder-to-liquid (P/L) ratios were mixed for 60 s in a ceramic bowl at 25 °C. For the injectability test, cement pastes were transferred into a 2 mL syringe with an 18 G (diameter: 1.2 mm) needle and subjected to axial pressure at 15 mm/min. An assembled fixture was used to fix the syringe. The inject force and displacement curves were recorded. The cement was injected into a flask filled with simulated body fluid and then incubated at 37 °C in a shaking incubator at 100 rpm. The images before and after shaking for 15 min were captured.

For the setting time test, the pastes were transferred into Teflon molds (d = 6 mm, h = 12 mm). The setting time was determined by a Vicat needle with a 1.0 mm diameter and a 400 g load cell according to ISO 9917 (2007). The samples with a 6 mm diameter and a 12 mm height were used for the compressive strength test. After curing, the cement samples were de-molded and subsequently cured under 37 °C and 100% humidity. Samples at different time points (3, 7, 21 days) were tested directly using an electronic universal testing machine (CM4305, MTS, China) with a 5 kN load cell and 5 mm/min loading speed. For cement hydration in SBF, the de-molded samples were immersed in SBF (Coolaber, China). After 7 days the compressive strength was directly evaluated under the same conditions with six samples analyzed in each group. Once tested, the samples were immersed in isopropyl alcohol (AR, Macklin, China) to cease the hydration reaction and subsequently ground for XRD analysis. The ground samples were examined by XRD using Cu Ka radiation (40 kV, 40 mA) in a continuous scanning mode. The quantitative analysis of the obtained XRD data was carried out by the Rietveld method using the Highscore Plus software. For SEM operation (IT-200, Japan), the cross-section of TMPC was sprayed with gold. The EDS spectra were obtained using a large area XMax silicon drift EDS detector (Oxford Instruments, UK) and analyzed via the software Aztec (Oxford Instruments, UK).

Mercury intrusion porosimetry (MIP) was used to characterize the porosity and pore distribution of hydrated samples after 3 days with a mercury porosimeter (AutoPore IV 9500, Micromeritics, USA). The pressure was increased to 420 kPa during the analysis and then rapidly decreased to 0 kPa. The internal software of the porosimeter determines the results with a contact angle of 130°.

2.3. Suspension experiment of TMPC

The pH and conductivity of the cement suspension were measured by a multi-parameter controller (DZS-706, INESA, China). The pH, conductivity and temperature probes were first calibrated before being inserted into the water until the parameters stabilized. Then, 12 g powders were poured into 60 mL water (powder-to-liquid ratio 5) under constant stirring at room temperature. The cement paste was sealed with plastic wrap to inhibit carbonation and water evaporation. The reaction was monitored for 24 h, with data recorded every 10 s during the first 2 h and the last 1 h. The cement paste at different reaction stages was collected and soaked in isopropanol (AR, Macklin, China) to stop the hydration reaction. The cement paste was then washed with isopropanol several times and dried overnight in a vacuum oven at 45 °C. The obtained cement samples were analyzed by XRD and thermos gravimetric analysis (TGA, STA2500, Retsch, Germany). The TGA was carried from 50 to 600 °C at 10 °C/min under a nitrogen atmosphere. The quantitative analysis of the obtained XRD data was carried out by the Rietveld

method using the Highscore Plus software.

2.4. Hydration temperature measurement

The hydration temperature was recorded by a digital temperature and humidity data logger (GSP-6, Elitech, China). Briefly, cement powder was mixed with water for 60 s and then transferred into a 5 mL centrifuge tube. A type-K thermocouple was set in the middle of the cement paste and the data was recorded every 10 s.

2.5. Degradation rate and pH value measurement

After curing, the cement disks were vacuum dried at 40 °C overnight and the initial mass (m_i) was recorded. The disks were then immersed in 0.05 M Tris-HCl buffer (pH = 7.4) at 0.2 g/mL. The buffer was refreshed every 3 days and the pH value was recorded at each time point by the multi-parameter analyzer. The masses m_d of disks were weighed after washing and vacuum drying. The weight loss ratio was calculated as $\frac{m_i - m_d}{m_i} \times 100\%$.

2.6. Operability study of TMPC

To evaluate the filling performance of bone cement for irregular defects, the bone cement was injected into the lab-made resin mold with irregular cavities. After curing, the mold was cut open and the cross section image was captured. We evaluated the filling performance and cement leakage in the human vertebra created by 3D printed models and fresh porcine cadaver vertebra purchased from the local market. The printed vertebra was cut transversely and filled with foam to create gaps and cavities. Bone cement was then injected from the pedicle. A 2 mm diameter and 40 mm depth hole in the pedicle of the porcine vertebra was drilled, followed by the injection of the cement. After curing, the vertebral body was scanned by computed tomography (CT). Standard scan settings were used (peak voltage of 100 kV, tube current of 100 mA) and images were reconstructed (slice thickness of 0.5 mm). The original data was analyzed by Mimics software.

2.7. In vitro cytocompatibility evaluation

After hydration for three days, the samples were extracted according to ISO 10993–5. Briefly, cement samples were extracted by alpha minimal essential medium (α-MEM, Cytiva, USA) at the concentration of 0.2 g/mL for 24 h at 37 °C. The extracts were filtered by a 0.22 μm filter and mixed with 10% fetal bovine serum (FBS, Gibco, USA) and 1% penicillin and streptomycin (P. S., Gibco, USA). Bone marrow mesenchymal stem cells (BMSCs) isolated from rats were cultured in 90% α-MEM with 10% FBS and 1% P. S. at 37 °C with 5% CO_2. BMSCs at passages 2–6 were used in this study. 2×10^3 cells/well were added into 96-well plates. After 8 h, the medium was replaced by extracts. The extracts were changed every 2–3 days. The cell viability was detected by the cell counting kit-8 (CCK-8, Yeasen, China) method after culturing for 24, 72, and 120 h. For live and dead staining, 10^4 cells were seeded on the disk samples (Φ8 mm × 2 mm) curing for 3 days in a 48-well plate. After 3 days, Calcein-AM/PI Double Stain Kit (Yeasen, China) was used. The cells were observed by a fluorescence microscope (Olympus IX71).

2.8. Statistical analysis

Results are expressed as the mean and standard deviation (SD). Comparative studies of means were performed by one-way analysis of variance (ANOVA) with a statistical significance at $p < 0.05$ (*$p < 0.05$, **$p < 0.01$, ***$p < 0.0001$).

3. Results and discussion

3.1. Rational design of TMPC

In our TMP-KDP-H_2O system, TMP and KDP could react in an equal molar ratio (mass ratio of 1.93:1) and produce K-struvite and newberyite ($MgHPO_4 \cdot 3H_2O$) as shown in Eq. (1). In the constructed ternary phase diagram in mass ratio (Fig. 1b), three regions corresponding to TMP insufficient, KDP insufficient and H_2O insufficient zones were obtained by connecting the theoretical reaction points with the vertices. Considering the hydration reaction, operating and cement performance of MPC, the components are usually designed under conditions of insufficient KDP or H_2O [19]. In the MPC system, the reaction degree of MgO or $Mg_3(PO_4)_2$ and the performance of cement can be regulated by two factors, magnesium to phosphate (M/P) ratio and powder to liquid (P/L) ratio. We conducted a comprehensive study on bone cement proportioning and the recipes of TMPC are shown in the diagram (Fig. 1b; Table S1). In the formulation design, we ensured the sufficient content of TMP and studied different properties of the cement by adjusting the M/P ratio and P/L ratio. The XRD pattern, average particle size and specific surface area of the powders used in this study are shown in Fig. S1, Fig. S2 and Table S1. The element purity of TMPC and KDP were shown in Table S3 and Table S4. The details of the study are shown as follows.

$$Mg_3(PO_4)_2 + KH_2PO_4 + 12H_2O \rightarrow MgKPO_4 \bullet 6H_2O + 2MgHPO_4 \bullet 3H_2O \quad (1)$$

3.2. Setting time, compressive strength, and injectability study of TMPC

The setting time was prolonged with the decrease of M/P ratio and the increase of P/L ratio (Fig. S3). The longest setting time occurred at M/P ratio 2, which varied from 41.83 to 23.41 min with the rise of P/L ratio from 2.0 to 3.0 g/mL. With the increase of P/L ratio, the setting time decreased rapidly, ranging from 17.75 to 13.75 min at M/P ratio 3 and 8.58 to 6.33 min at M/P ratio 4, respectively. Though a long setting time benefits the surgical process, it may also affect the patient's recovery after surgery [10]. It is worth noting that the operation temperature also affects the curing speed of K-struvite cement [18]. In this study, we tested the setting time at room temperature, while the actual curing time would be shorter once the cement is injected into the body.

The compressive strength increased continuously with the prolonged hydration time for all cement samples. At a low P/L ratio (2.0 g/mL), all TMPC samples continued to react and maintained a high strength growth rate in 7–21 days (Fig. 2b; Fig. S4a, Fig. S5a). The highest strength was observed at M/P ratio of 3 and P/L ratio of 3.0, and the compressive strength was 94.1 ± 40.2, 122.1 ± 17.9, and 145.0 ± 22.5 MPa after 3, 7, and 21 days of hydration, respectively. Generally, an increase in the M/P ratio (i.e. TMP content) led to a corresponding increase in the compressive strength. The excessive TMP could ensure a sufficient reaction of KDP and also function as an aggregate to augment the strength of bone cement [25]. Increasing the P/L ratio is also a typical strategy to enhance the cement strength. Our findings indicated that a high P/L ratio could enhance the strength and facilitate rapid strength development. Indeed, when the P/L ratio was 3.0, all TMPC samples achieved a high strength in the first 7 days with insignificant strength gains (less than 20%) from 7 to 21 days. Water content reduction in the cement will lead to its decreased porosity and increased density, which plays a crucial role in improving its strength. Therefore, a high P/L ration should be employed to achieve high strength and rapid strength development. Furthermore, we assessed the influence of SBF on the compressive strength of bone cement by immersing the cured bone cement in SBF, with subsequent testing of the compressive strength after 7 days (Fig. S6). At a P/L ratio of 3.0, the compressive strength of TMPC-2, TMPC-3 and TMPC-4 was 40.0 ± 6.4, 85.6 ± 12.4 and 62.9 ± 11.5 MPa, respectively. The compressive strength attenuation in SBF

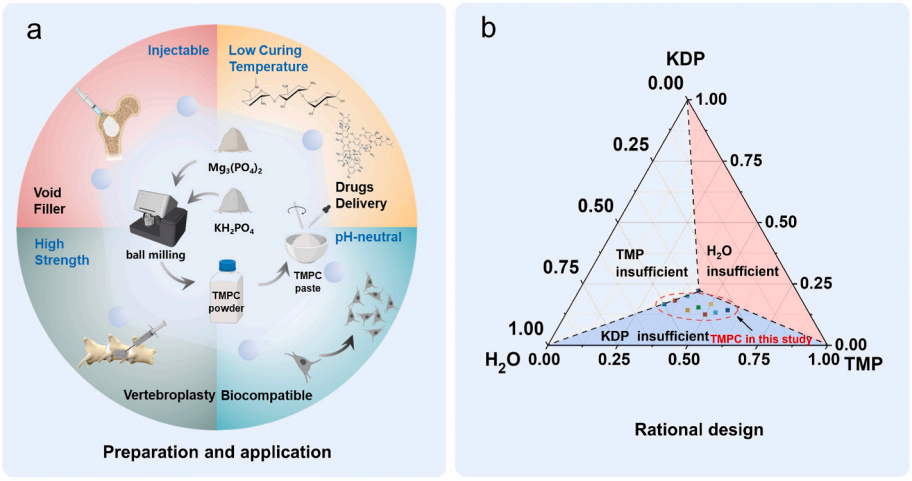

Fig. 1. Design and application of our high-strength trimagnesium phosphate cement. a) Preparation and application of TMPC. TMPC has the properties of injectability, low curing temperature, high strength, and neutral pH, which can be used as bone void filler, drug carrier, and bone cement for vertebroplasty. b) Ternary phase diagram in mass ratio of TMPC.

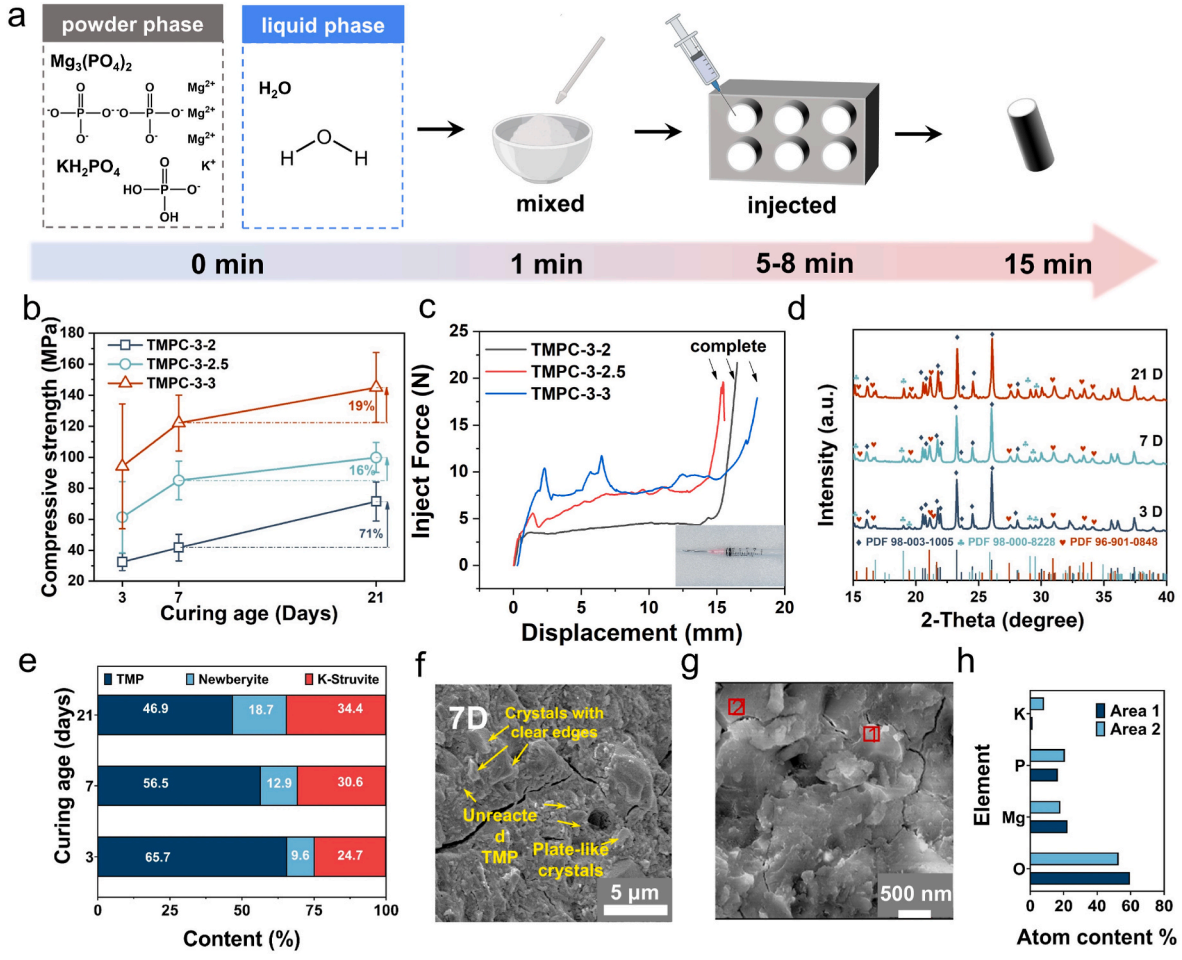

Fig. 2. Compressive strength, injectability and hydration product of TMPC. a) Preparation of TMPC samples. b) Strength development of TMPC. c) Inject force of TMPC-3. d) Hydration product of TMPC-3 (TMP: PDF 98-000-8228, Newberyite: PDF 96-901-0848, K-Struvite PDF 98-003-1005). e) Content of the hydration product; f), g) and h) Cross-section morphology, EDS analysis of TMPC-3 after hydration for 7 days, respectively.

decreased with increasing M/P ratio and was most pronounced at an M/P ratio of 2.0. This phenomenon could be attributed to the porosity and hydration products of the TMPC, which will be discussed further in the subsequent sections.

To ensure an optimal injectability of TMPC, it is essential to maintain a certain level of water content. Thus, we conducted a comprehensive investigation of the injectability by varying the M/P and P/L ratios. We used a universal testing machine to record the injection force curves and

analyzed the injectability. Our results indicated that most samples demonstrated prolonged plateau periods, corresponding to good injectability (Fig. 2c; Figs. S4b and S5b) [26]. However, the injectability decreased with the increase of M/P ratio and P/L ratio. Notably, at P/L ratios of 2.0 and 2.5, the increase of M/P ratio did not affect the injectability but the injecting force. Moreover, even at P/L ratio 3.0, the injection force of TMPC-3 remained below 10 N and the cement could be completely injected (Fig. 2c). The stability of the TMPC paste was demonstrated by the absence of solid-liquid separation during the injection period [27]. After the injected cement was immersed in SBF and shaken at 37 °C for 15 min, no significant powder or dissolution was observed (Fig. S7), indicating the good anti-washout behavior of the cement.

3.3. Hydration product and microstructure study of TMPC

To achieve high strength and fast development, we set P/L ratio as 3.0 g/mL and detected the hydration products at different M/P ratios and hydration ages (Fig. 2d). Quantitative analysis was carried out to determine the content of each phase (Fig. 2e) and the weighted profile R-factor (R_{wp}) is shown in Table S5. After 3 days of hydration, the hydration product content of TMPC-3 was 9.6% for newberyite and 26.7% for K-struvite. After 21 days, the content of TMP, newberyite, and K-struvite was 46.9%, 18.7%, and 34.4%, respectively. The XRD data also reflected the hydration speed in the TMP-KDP-H_2O system (Fig. 2d; Figs. S4c and S5c). The results showed that increasing the M/P ratio led to more K-struvite formation at the early stage, indicating an acceleration in the reaction speed, which was consistent with the trend observed in the setting time and strength development of the system (Figs. S4d and S5d). The manipulation of the hydration products and reaction speed by M/P ratio may be related to the pH value. The high M/P ratio could increase the pH value in the TMPC system, leading to the rapid direct formation of K-struvite and inhibiting the further reaction of TMPC. This speculation was confirmed in the following suspension study.

We studied the cross-section morphologies of TMPC at P/L ratio of 3.0 (Fig. 2e; Fig. S8). The cracks could be observed, which may presumably be created during the drying of the hydrated gel-like phase and the evaporating of the free water [28,29]. The number and width of cracks decreased significantly with increasing aging time, suggesting that the reaction further consumes the free water. Three different morphologies could be observed, including crystals with clear edges, small irregular particles and plate-like crystals, and the different phases were further identified by energy dispersive spectroscopy (EDS). These crystals with clear edges were potassium-rich phases, which could be assigned to the K-struvite (Fig. 2g and h; Fig. S9). In general, these phase regions are accompanied by cracks resulting from the dehydration of K-struvite during drying. The small irregular particle and plate-like crystals are associated with potassium-poor phases, representing the unreacted TMP and newly formed newberyite [30,31]. With the increasing hydration age, the content of K-struvite increased while the unreacted TMP decreased, and the cement matrix binds more tightly. With the increase of M/P ratio, the number of crystals with clear edges decreased, which was related to the decrease in the component of K-struvite and the increase in the unreacted TMP. The number and width of the crack also reduced with the increasing TMP content, confirming the gradual decline in the proportion of K-struvite in the hydrated product. K-struvite, the main hydration product in TMPC cement, acts as a cementing phase to bond the unreacted TMP to the newly generated crystals, forming a continuous and homogeneous matrix structure [32]. These unreacted TMP phases could act as aggregate, improving the cement's strength [33]. The reasonable proportion and uniform distribution of these hydration products are crucial for the mechanical properties of the cement.

To delve deeper into the microstructure of TMPC, MIP was utilized to analyze the porosity and pore distribution of TMPC (Fig. S10, Table S7). The porosity of TMPC-2, TMPC-3 and TMPC-4 was 19.99%, 23.72% and 22.09%, respectively. Despite the higher porosity compared to MPC cement [34], the pore size distribution was relatively small. Specifically, the average pore diameter of TMPC-2, TMPC-3 and TMPC-4 was 92.23, 27.85 and 26.7 nm, respectively. Notably, the average pore diameter of TMPC was significantly lower than that of MPC or CPC. According to the reported theory, the strength of bone cement will be affected by pores with different diameters, while those pores with sizes less than 100 nm show little influence, which are known as harmless pores [35]. With the increase of M/P ratio, the content of pores above 100 nm significantly decreased, which played a vital role in enhancing the performance of bone cement [36]. Compared with the bone cement previously studied, TMPC exhibited relatively small pore sizes. This small pore diameter may contribute to the high compressive strength of TMPC. It is worth noting that although this pore structure can obtain high strength, it will negatively impact cell growth and liquid penetration. Our future work will focus on the in vivo evaluation of the bone repair properties of TMPC.

3.4. Hydration kinetic study of TMPC

The investigation of hydration kinetics is vital for determining the appropriate cement ratios and comprehending the rates and products of cement hydration reactions. To further clarify the in-situ phase transformation in TMPC with different M/P ratios, we monitored the hydration reaction at a P/L ratio of 0.05. We recorded the real-time variations in pH and conductivity curves, which indicated the ion release during the dissolution of TMPC in the cement suspension, and collected its intermediate products for thermogravimetric and XRD analysis (Fig. 3a). The phase content of each reaction stage was quantitatively analyzed by XRD and the weighted profile R-factor (R_{wp}) was shown in Table S6. Inflection in the pH value curves were observed due to the dissolution and precipitation reactions, as described by Eqs. (2)–(8) corresponding to possible phase changes [31]. Based on the pH value, conductivity, and XRD results, we proposed two processes of cement formation.

We first conducted the suspension experiment at M/P ratio of 3.0. The first stage was the dissolution of raw powders and the formation of newberyite. Upon the addition of powder to water, the pH value dropped rapidly and then increased (Fig. 3b). In the initial reaction stage, the rapid dissolution of KDP resulted in the release of K^+ and $H_2PO_4^-$ and a corresponding rapid increase in conductivity. A distinct pH decrease was observed at P1 (5.8 min), suggesting a possible transformation. We collected the powders at 5.8 min, and the XRD result showed the presence of newberyite at that stage as well as the absence of KDP, indicating the almost dissolution of KDP powder (Fig. 3c and d). Derivative thermogravimetry (DTG) and thermogravimetry (TG) curves could reflect the weight loss of the samples at different time points (Fig. 3e). The observed DTG peak at 96 °C could be related to the decomposition of newberyite. The mass loss between 50 and 200 °C is 7.95%. These results demonstrate that newberyite is the only hydration product (Eq. (2) and (3)).

Stage I:

$$Mg_3(PO_4)_2 + H_2PO_4^- + 10H_2O \rightarrow 3MgHPO_4 \bullet 3H_2O + OH^- \quad (2)$$

$$Mg_3(PO_4)_2 + HPO_4^{2-} + 11H_2O \rightarrow 3MgHPO_4 \bullet 3H_2O + 2OH^- \quad (3)$$

The second stage was the phase transformation and the direct formation of K-struvite. A sharp electrical conductivity drop was observed after P1, and the hydration product at P2 (28.6 min) was collected, representing the reaction product before that time. The XRD results showed that magnesium potassium hydrogen phosphate hydrate (HP: $Mg_2KH(PO_4)_2{\cdot}15H_2O$) was the main product, and no newberyite was detected (Fig. 3c). A portion of K-struvite has also been detected at that stage. According to DTG curves (Fig. 3d), only a broad peak at around

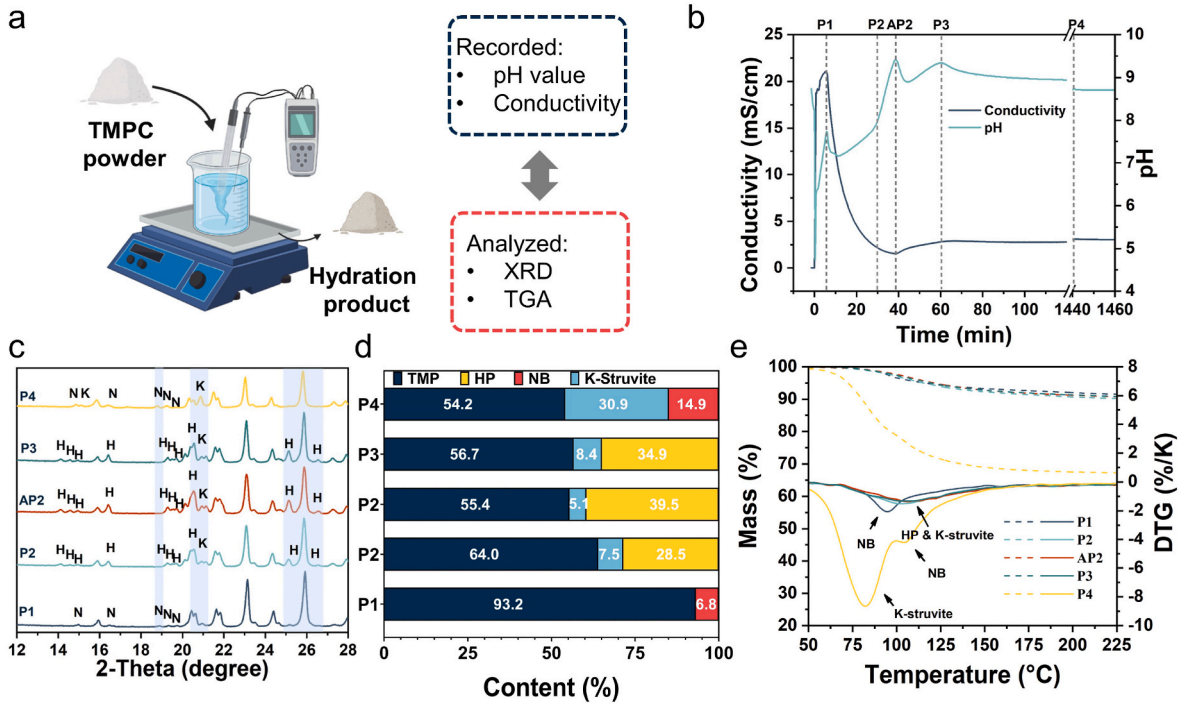

Fig. 3. Suspension experiment of TMPC. a) The process of suspension experiment: The pH value and conductivity were recorded. Then, the hydration product was collected and analyzed by XRD and TGA. b) pH and conductivity curves. c) XRD patterns of the hydration product. d) Content of the hydration product. e) DTG and mass loss of hydration product. (TMP: $Mg_3(PO_4)_2$, HP: $Mg_2KH(PO_4)_2{\cdot}15H_2O$ NB: $MgHPO_4{\cdot}3H_2O$, K-Struvite: $MgKPO_4{\cdot}6H_2O$) (P1 = 5.8 min, P2 = 30 min, AP2 = 38 min, P3 = 60 min, P4 = 1440 min).

105 °C was detected, which could be assigned to the decomposition of K-struvite and HP. Two possible reactions may occur based on the product generated in this stage. The first was a transformation from newberyite to HP (Eq. (4)), and the second was a reaction between TMP and K^+, leading to the HP formation (Eq. (5)). Both reactions released hydrogen ions, which resulted in a pH decrease. We also observed a slope change in the pH values at P2. As no newberyite was detected at that stage (before P2) and the hydration products were HP and K-struvite, the complete transformation of the newberyite was speculated to decrease the generation rate of H^+, and most reactions might decrease the system's pH (Eq. (4), (5) and (8)). The pH value was also related to the ionization of phosphoric acid [37]. At that stage (P1–P2), the phosphoric acid was dominated by second ionization, and the formation of HP followed Eq. (6). The OH^- generated from HP formation increased the pH value. According to the XRD results, the intensity of HP reached the highest (39.5%) at AP2. A decrease in pH was observed at this time point, probably due to the consumption of OH^- by transformation from HP to K-struvite (Eq. (7)). Besides, an increase in conductivity could also be observed, probably attributed to HP's dissolution [38]. At the same time, from the results of XRD, the content of HP decreased by 5.4%, while that of K-struvite increased by 3.3%. After P3, the pH decreased gently and the conductivity became stable, the direct generation of K-struvite and transformation of HP continually consumed the ions in the suspension (Eq. (8)). The similar DTG curves at P2, AP2 and P3 showed similar components and the mass loss of these time points shows no significant differences. No HP was detected after 24 h (P4), suggesting a complete transformation of HP to K-struvite. The mass loss (50–200 °C) at P4 reached 32.49%, relating to the decomposition of newberyite and K-struvite. Newberyite was detected after 24 h, demonstrating the sufficient hydration reaction as Eq. (1) (Fig. 3c).

Stage II:

$$2MgHPO_4 \bullet 3H_2O + K^+ + 9H_2O \rightarrow Mg_2KH(PO_4)_2 \bullet 15H_2O + H^+ \quad (4)$$

$$2Mg_3(PO_4)_2 + 3K^+ + 2H_2PO_4^- + 45H_2O \rightarrow 3Mg_2KH(PO_4)_2 \bullet 15H_2O + 3H^+ \quad (5)$$

$$2Mg_3(PO_4)_2 + 3K^+ + 2HPO_4^{2-} + 46H_2O \rightarrow 3Mg_2KH(PO_4)_2 \bullet 15H_2O + OH^- \quad (6)$$

$$Mg_2KH(PO_4)_2 \bullet 15H_2O + K^+ + OH^- \rightarrow 2MgKPO_4 \bullet 6H_2O + 4H_2O \quad (7)$$

$$Mg_3(PO_4)_2 + 3K^+ + HPO_4^{2-} + 18H_2O \rightarrow 3MgKPO_4 \bullet 6H_2O + H^+ \quad (8)$$

As a control, at M/P ratio 4, the pH value rose rapidly after the powder contacted with water, and the pH value reached the highest at 25.6 min (Fig. S11a). We found the direct crystallization of K-struvite at P1, which was the only hydration product (Figs. S11b and S11c). From 50 to 210 °C, the loss of crystallization water of K-struvite is mainly observed. According to the TG-DTG curve, the weight loss rate increased in the P1–P2 stage, indicating the continuous generation of MKP, but the subsequent change was not noticeable (Fig. S11d; Table S6). After 1440 min, the content of K-struvite increased significantly to 31.3%. However, another hydration product $Mg_3(PO_4)_2{\cdot}22H_2O$ (cattiite) was observed in the suspension experiment. The formation of cattiite may be related to the high pH and P/L ratio [39]. The weight loss was 27.07% at P4, mainly due to the large amount of crystalline water in cattiite. While at M/P ratio 2, the first pH-decreasing point P1 occurred at 20 min, and the pH change range was insignificant (Fig. S12a). Compared to the other groups, the hydration proceeded slower. The pH value was maintained at 6–7 before 100 min, and the conductivity decrease was insignificant. The hydration product was newberyite and K-struvite (Figs. S12b and S12c). It is worth noting that the content of TMP in TMPC-2 was lower than that of TMPC-3 and TMPC-4 in each hydration stage, and the TG results showed that a large amount of water was formed during the hydration (Fig. S12d and Table S8). With a high KDP content, the system's initial pH was low, causing a rapid dissolution of TMP. However, at that pH value, the reaction driving force was

insufficient. Through the pH and conductivity curves, the precipitation processed slower compared to M/P = 3.0 and 4.0. A high conductivity remains before 40 min (Fig. S12a). This phenomenon led to the long curing time of TMPC-2. After 1440 min, the pH value reached 8.5 and the conductivity reached 4.7 mS/cm, indicating that the reaction was almost complete.

These results illustrated the critical role of M/P ratio in the cement hydration process. The actual reaction process of MPC is intricate and involves a range of established theories [40], including a homogeneous nucleation mechanism [41], a heterogeneous nucleation mechanism [42], and multiple precipitation/dissolution reactions [39]. The suspension study demonstrated that the TMPC system fits well with the multiple precipitation/dissolution reaction theory. We have developed a hydration schematic for the TMP-KDP-H_2O system (Fig. 4). Throughout the reaction process, the dissolution of TMP leads to an increased pH value, which is the driving force and may determine the dominant reaction. Under a low pH value (about 7), $MgHPO_4{\cdot}3H_2O$ formation is the dominant reaction and the hydration process progresses gently. The transformation starts when pH rises and mixed phases forms, including newberyite, HP, and K-struvite. The hydration accelerates when the pH reaches about 8, with HP and K-struvite as the primary product, followed by the final transformation of HP to K-struvite. Rising the M/P ratio value could influence the hydration routine by increasing the systems' pH and promoting the direct formation of K-struvite. Based on the above mechanism, it may be possible to regulate the properties of TMPC by adjusting the pH of the reaction system with a certain M/P ratio. For instance, adding an acid retarder to delay the increase of pH in the early hydration process may be an effective approach to regulate the hydration rate of TMPC further. These investigations provide a scientific foundation for rational design and performance control of TMPC cement.

3.5. Application of TMPC cement

From an application perspective, we evaluated the hydration temperature, degradation ratio and pH, the in vitro biocompatibility, and injectability (Fig. 5). As shown in Fig. 5a, compared with the high hydration temperature of PMMA (>90 °C), the peak temperature for TMPC-3 was extremely low (38.8 °C). There was a rapid heat generation for PMMA at around 10 min, although the initial heat release was insignificant. In contrast, TMPC-3 showed a rapid heat generation rate after injection, but the subsequent heat was released smoothly. To evaluate whether the strength of TMPC can meet the needs of clinical use, we compared the strength properties of TMPC with PMMA bone cement commonly used in clinic and CPC bone cement. TMPC (M/P ratio 3 and P/L ratio 3.0 g/mL) possessed the highest early compressive strength (94 MPa at day 3), higher than the international standard of ISO 5833 and similar to the commercial PMMA bone cement (Osteopal@ V) (Fig. 5b) [25,34,43,44].

Another advantage of TMPC over PMMA is its degradation property. The degradation experiment was conducted for 28 days, and the degradation rate reached 12% after 28 days. With the increase of M/P ratio, the degradation rate slows down because the dissolution rate of struvite is greater than that of TMP [32]. Worth mentioning, the degradation rate of TMPC is greater than that of MPC under the same M/P ratio because of the greater solubility of TMP than MgO. However, MPC bone cement usually has a low M/P ratio to obtain a low pH, so the relative content of struvite increases. Overall, the degradation rate of TMPC should be lower than that of MPC. During the whole degradation process, pH showed a trend of rising first and then falling. In the early degradation stage, the pH was 7.96. As degradation progressed, the pH dropped and stabilized at about 7.4 after 7 days. At a high M/P ratio, the maximum pH was maintained within 8, and the system was significantly less alkaline than conventional MPC.

We tested the cell viability of BMSCs and found that the extraction of both TMPC and PMMA after curing for 72 h had negligible toxicity to BMSCs. After 120 h, BMSCs maintained high cell viability (Fig. 5d). We also seeded the cells on hardened TMPC and PMMA plate samples and found that more cells could adhere to TMPC samples compared to PMMA. The cells lived in good condition in both samples and could spread, though only a few died (Fig. 5e).

To better study the filling capacity of TMPC, we selected three

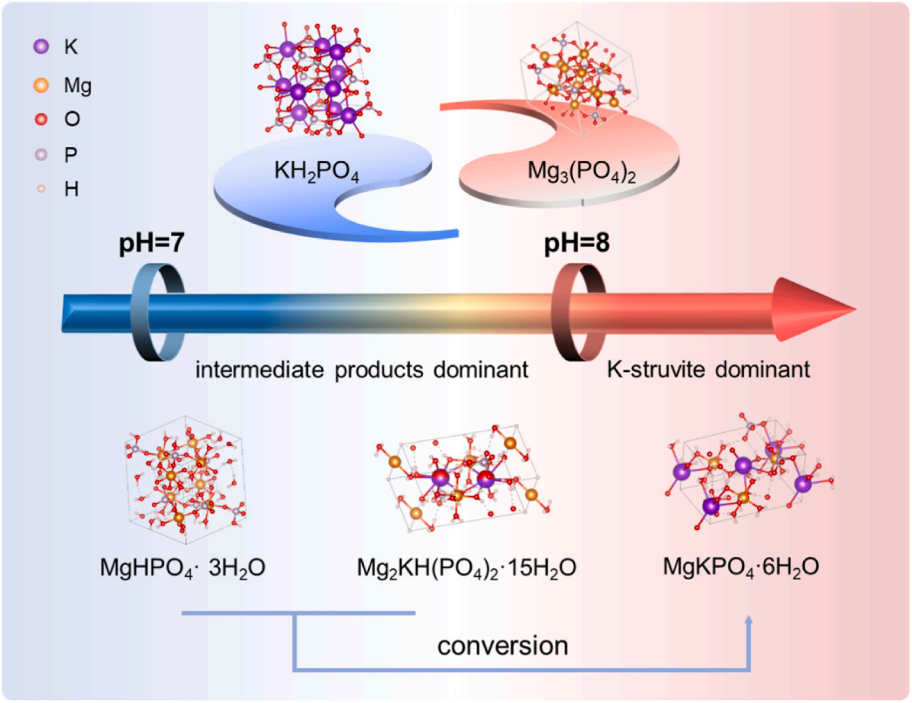

Fig. 4. Schematic diagram of TMPC cement hydration process. The pH value of the system determines the reaction process. $MgHPO_4{\cdot}3H_2O$ forms at pH around 7. With the increase of pH value, the formation of $MgHPO_4{\cdot}3H_2O$ is inhibited and it transformed to K-struvite. The intermediate product $Mg_2K(HPO_4)_2{\cdot}15H_2O$ forms at pH about 8. With further pH increase, the $Mg_2K(HPO_4)_2{\cdot}15H_2O$ content reaches the highest and transforms to K-struvite.

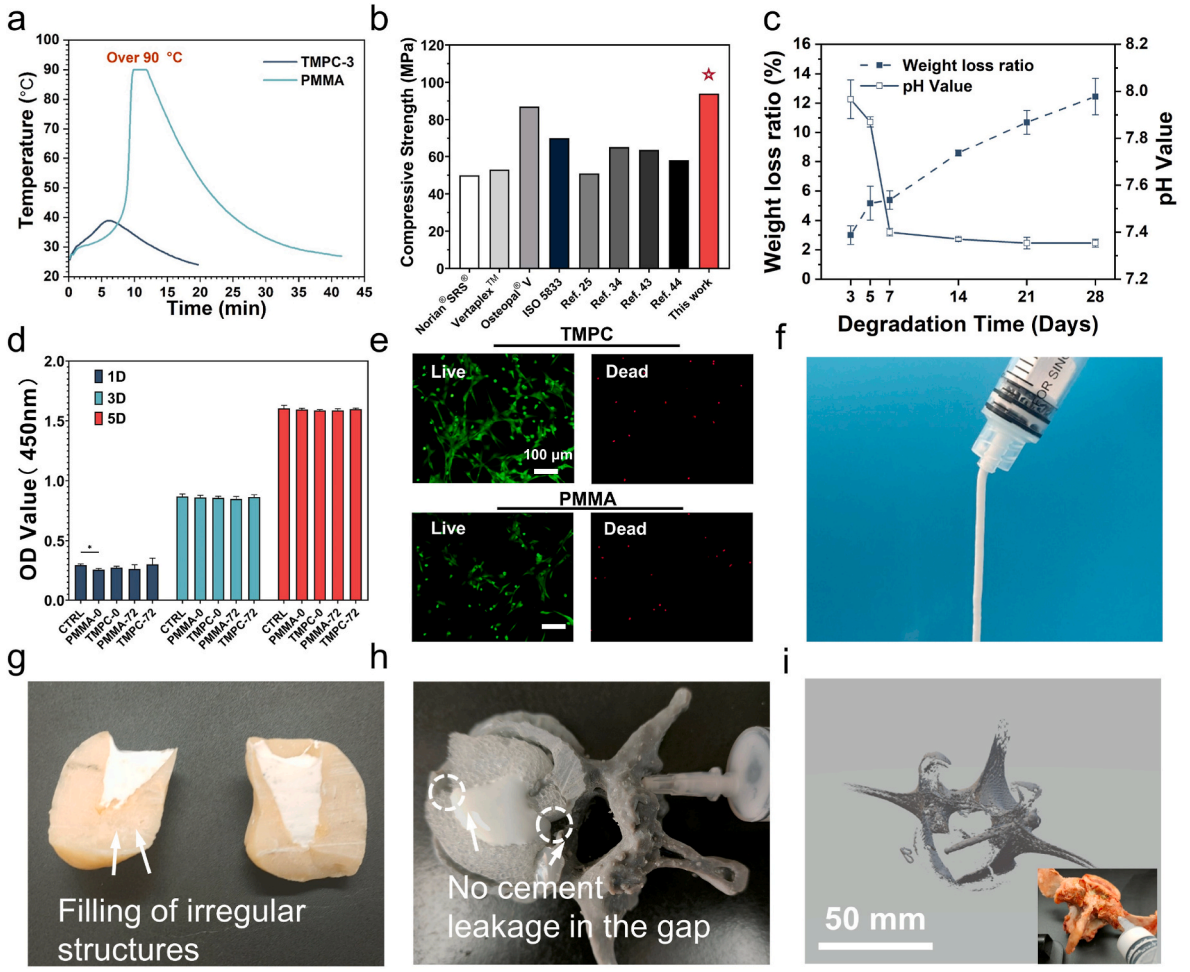

Fig. 5. Application performance study of TMPC. a) Hydration temperature of TMPC-3 and PMMA. b) Comparison of the compressive strength to the commercial and recently researched bone cements. c) Degradation ratio and pH value. d) Cell viability after culturing with the extract. d) Live and dead staining of BMSCs seeded on TMPC-3 and PMMA after 3 days (*$p < 0.05$). f) Injectability study of TMPC-3. g) Filling performance of TMPC for irregular models. h) The filling and leakage performance of the TMPC was evaluated using a 3D-printed human vertebral body model. i) The spine was reconstructed by CT after injection of bone cement.

models, including the mold with an irregular structure, the 3D printing model of the human vertebral body, and the porcine spine bones. TMPC could fill in the mold, and even the irregular corners, confirming its good injectability and flowability (Fig. 5f and g). Using an incised 3D printing vertebral body model, we created a cavity and a gap after filling both sides with foam. After injection, no significant leakage was observed in the gap, and the cement was evenly distributed in the cavity (Fig. 5h). TMPC was also injected into the pre-drilled vertebrae (Fig. 5i). Though only the working channel was created, the good distribution of the cement in the channel could be observed by reconstructed CT morphology (Fig. 5i). The cadaver vertebrae study further proved the good injectability and filling performance of the TMPC, which can be successfully used in percutaneous vertebroplasty/percutaneous kyphoplasty procedures or other bone defect filling. These results suggest that TMPC showed outstanding clinical application capability and could serve as a future alternative to PMMA.

4. Conclusion

This study has developed a superior bone cement system (TMPC) that surpasses the performance capabilities of traditional MPCs. By replacing MgO with TMP, the TMPC exhibited improved compressive strength, reduced pH value and heat release. TMPC possesses good injectability, and the compressive strength could reach 94 MPa after hydration for 3 days. In addition, we have conducted a detailed study on the hydration kinetics of the TMP-KDP-H_2O system and succeed in understanding the phase transformation during the hydration under different M/P ratios. A low M/P ratio led to a gentle hydration and the formation of newberyite and K-struvite. Increasing the M/P ratio resulted in the direct generation of K-struvite, accelerating the hydration process. By regulating M/P ratio, the hydration process can be controlled, and the properties of cement can be affected. The results of this work will be conducive to the design and comprehension of high-performance MPC cement, which represents a step forward for MPCs in the biomedical field.

Ethics approval and consent to participate

Animal or human experiments are not involved in this study.

Declaration of competing interest

The authors declare that they have no known competing financial interests or personal relationships that could have appeared to influence the work reported in this paper.

Acknowledgments

This work was supported by grants from The National Key Research and Development Program of China (2022YFB4601402), the National Natural Science Foundation of China (32201109 , 51772233,

51861145306), the Guangdong Basic and Applied Basic Research Foundation (2022B1515120052, 2021A1515110557), and the Self-innovation Research Funding Project of Hanjiang Laboratory (HJL202202A002). The authors acknowledge the technical support of Dr. Honglei Kang from Tongji Medical College of Huazhong University of Science and Technology and Dr. Liangliang Huang from Central Hospital of Central Theater Command.

Appendix A. Supplementary data

Supplementary data to this article can be found online at https://doi.org/10.1016/j.bioactmat.2023.05.019.

References

[1] M.S. Kang, N.H. Lee, R.K. Singh, N. Mandakhbayar, R.A. Perez, J.H. Lee, H.W. Kim, Nanocements produced from mesoporous bioactive glass nanoparticles, Biomaterials 162 (2018) 183–199, https://doi.org/10.1016/j.biomaterials.2018.02.005.

[2] W.A. Jiranek, A.D. Hanssen, A.S. Greenwald, Antibiotic-loaded bone cement for infection prophylaxis in total joint replacement, J. Bone Joint Surg. 88 (11) (2006) 2487–2500, https://doi.org/10.2106/JBJS.E.01126.

[3] E. Jacobs, K. Saralidze, A.K. Roth, J.J.A. de Jong, J.P.W. van den Bergh, A. Lataster, B.T. Brans, M.L.W. Knetsch, I. Djordjevic, P.C. Willems, L.H. Koole, Synthesis and characterization of a new vertebroplasty cement based on gold-containing PMMA microspheres, Biomaterials 82 (2016) 60–70, https://doi.org/10.1016/j.biomaterials.2015.12.024.

[4] G. Lewis, Injectable bone cements for use in vertebroplasty and kyphoplasty: state-of-the-art review, J. Biomed. Mater. Res. B: Applied Biomaterials 76B (2) (2006) 456–468, https://doi.org/10.1002/jbm.b.30398.

[5] Y.J. No, S.I. Roohani-Esfahani, H. Zreiqat, Nanomaterials: the next step in injectable bone cements, Nanomedicine 9 (11) (2014) 1745–1764, https://doi.org/10.2217/nnm.14.109.

[6] J.J. Verlaan, M.A. Lopez-Heredia, J. Alblas, F.C. Oner, J.A. Jansen, W.J.A. Dhert, 7.12 Injectable Bone Cements for Spinal Column Augmentation: Materials for Kyphoplasty/Vertebroplasty, Comprehensive Biomaterials II, 2017, pp. 199–215, https://doi.org/10.1016/B978-0-12-803581-8.10230-9.

[7] C. Robo, G. Hulsart-Billström, M. Nilsson, C. Persson, In vivo response to a low-modulus PMMA bone cement in an ovine model, Acta Biomater. 72 (2018) 362–370, https://doi.org/10.1016/j.actbio.2018.03.014.

[8] J. Zhang, W. Liu, V. Schnitzler, F. Tancret, J.-M. Bouler, Calcium phosphate cements for bone substitution: Chemistry, handling and mechanical properties, Acta Biomater. 10 (3) (2014) 1035–1049, https://doi.org/10.1016/j.actbio.2013.11.001.

[9] H. Zhou, C. Liang, Z. Wei, Y. Bai, S.B. Bhaduri, T.J. Webster, L. Bian, L. Yang, Injectable biomaterials for translational medicine, Mater, Today Off. 28 (2019) 81–97, https://doi.org/10.1016/j.mattod.2019.04.020.

[10] M. Nakano, N. Hirano, M. Zukawa, K. Suzuki, J. Hirose, T. Kimura, Y. Kawaguchi, Vertebroplasty using calcium phosphate cement for osteoporotic vertebral fractures: study of outcomes at a minimum follow-up of two years, Asian Spine J 6 (1) (2012) 34, https://doi.org/10.4184/asj.2012.6.1.34.

[11] N. Ostrowski, A. Roy, P.N. Kumta, Magnesium phosphate cement systems for hard tissue applications: a review, ACS Biomater. Sci. Eng. 2 (7) (2016) 1067–1083, https://doi.org/10.1021/acsbiomaterials.6b00056.

[12] J.L. Wang, J.K. Xu, C. Hopkins, D.H. Chow, L. Qin, Biodegradable magnesium-based implants in orthopedics-A general review and perspectives, Adv. Sci. 7 (8) (2020), 1902443, https://doi.org/10.1002/advs.201902443.

[13] L. Wu, F. Feyerabend, A.F. Schilling, R. Willumeit-Römer, B.J.C. Luthringer, Effects of extracellular magnesium extract on the proliferation and differentiation of human osteoblasts and osteoclasts in coculture, Acta Biomater. 27 (2015) 294–304, https://doi.org/10.1016/j.actbio.2015.08.042.

[14] S. Lin, G. Yang, F. Jiang, M. Zhou, S. Yin, Y. Tang, T. Tang, Z. Zhang, W. Zhang, X. Jiang, A magnesium-enriched 3D culture system that Mimics the bone development microenvironment for vascularized bone regeneration, Adv. Sci. 6 (12) (2019), 1900209, https://doi.org/10.1002/advs.201900209.

[15] Y. Zhang, J. Xu, Y.C. Ruan, M.K. Yu, M. O'Laughlin, H. Wise, D. Chen, L. Tian, D. Shi, J. Wang, S. Chen, J.Q. Feng, D.H.K. Chow, X. Xie, L. Zheng, L. Huang, S. Huang, K. Leung, N. Lu, L. Zhao, H. Li, D. Zhao, X. Guo, K. Chan, F. Witte, H. C. Chan, Y. Zheng, L. Qin, Implant-derived magnesium induces local neuronal production of CGRP to improve bone-fracture healing in rats, Nat. Med. 22 (10) (2016) 1160–1169, https://doi.org/10.1038/nm.4162.

[16] N. Zheng, J. Xu, Y.C. Ruan, L. Chang, X. Wang, H. Yao, J. Wang, R. Zhang, Q. Xue, N. Tang, T.-y. Ong, J. Schilcher, R.J. O'Keefe, L. Qin, Magnesium facilitates the healing of atypical femoral fractures: a single-cell transcriptomic study, Mater. Today 52 (2022) 43–62, https://doi.org/10.1016/j.mattod.2021.11.028.

[17] L.J. Gardner, S.A. Walling, S.M. Lawson, S. Sun, S.A. Bernal, C.L. Corkhill, J. L. Provis, D.C. Apperley, D. Iuga, J.V. Hanna, N.C. Hyatt, Characterization of and structural insight into struvite-K, $MgKPO_4.6H_2O$, an analogue of struvite, Inorg. Chem. 60 (2021) 195–205, https://doi.org/10.1021/acs.inorgchem.0c02802.

[18] S.A. Walling, J.L. Provis, Magnesia-based cements: a journey of 150 Years, and cements for the future? Chem. Rev. 116 (2016) 4170–4204, https://doi.org/10.1021/acs.chemrev.5b00463.

[19] H. Ma, B. Xu, Potential to design magnesium potassium phosphate cement paste based on an optimal magnesia-to-phosphate ratio, Mater. Des. 118 (2017) 81–88, https://doi.org/10.1016/j.matdes.2017.01.012.

[20] G. Mestres, M. Abdolhosseini, W. Bowles, S.H. Huang, C. Aparicio, S.U. Gorr, M. P. Ginebra, Antimicrobial properties and dentin bonding strength of magnesium phosphate cements, Acta Biomater. 9 (2013) 8384–8393, https://doi.org/10.1016/j.actbio.2013.05.032.

[21] M.A. Goldberg, P.A. Krohicheva, A.S. Fomin, D.R. Khairutdinova, O.S. Antonova, A.S. Baikin, V.V. Smirnov, A.A. Fomina, A.V. Leonov, I.V. Mikheev, N.S. Sergeeva, S.A. Akhmedova, S.M. Barinov, V.S. Komlev, Insitu magnesium calcium phosphate cements formation: from one pot powders precursors synthesis to in vitro investigations, Bioact. Mater. 5 (2020) 644–658, https://doi.org/10.1016/j.bioactmat.2020.03.011.

[22] L. Yu, K. Xia, C. Gong, J. Chen, W. Li, Y. Zhao, W. Guo, H. Dai, An injectable bioactive magnesium phosphate cement incorporating carboxymethyl chitosan for bone regeneration, Int. J. Biol. Macromol. 160 (2020) 101–111, https://doi.org/10.1016/j.ijbiomac.2020.05.161.

[23] M. Schamel, J.E. Barralet, M. Gelinsky, J. Groll, U. Gbureck, Intrinsic 3D prestressing: a new route for increasing strength and improving toughness of hybrid inorganic biocements, Adv. Mater. 29 (35) (2017), https://doi.org/10.1002/adma.201701035.

[24] J. Wang, C. Liu, Y. Liu, S. Zhang, Double-network interpenetrating bone cement via in situ hybridization protocol, Adv. Funct. Mater. 20 (2010) 3997–4011, https://doi.org/10.1002/adfm.201000995.

[25] S. Yu, L. Liu, C. Xu, H. Dai, Magnesium phosphate based cement with improved setting, strength and cytocompatibility properties by adding $Ca(H_2PO_4)_2.H_2O$ and citric acid, J. Mech. Behav. Biomed. Mater. 91 (2019) 229–236, https://doi.org/10.1016/j.jmbbm.2018.12.004.

[26] W. Liu, J. Zhang, P. Weiss, F. Tancret, J.M. Bouler, The influence of different cellulose ethers on both the handling and mechanical properties of calcium phosphate cements for bone substitution, Acta Biomater. 9 (3) (2013) 5740–5750, https://doi.org/10.1016/j.actbio.2012.11.020.

[27] R. O'Neill, H.O. McCarthy, E.B. Montufar, M.P. Ginebra, D.I. Wilson, A. Lennon, N. Dunne, Critical review: injectability of calcium phosphate pastes and cements, Acta Biomater. 50 (2017) 1–19, https://doi.org/10.1016/j.actbio.2016.11.019.

[28] G. Mestres, M.P. Ginebra, Novel magnesium phosphate cements with high early strength and antibacterial properties, Acta Biomater. 7 (4) (2011) 1853–1861, https://doi.org/10.1016/j.actbio.2010.12.008.

[29] Z. Luo, Y. Ma, H. He, W. Mu, X. Zhou, W. Liao, H. Ma, Preparation and characterization of ferrous oxalate cement—a novel acid-base cement, J. Am. Ceram. Soc. 104 (2) (2020) 1120–1131, https://doi.org/10.1111/jace.17511.

[30] Y. Zhao, S. Yu, X. Wu, H. Dai, W. Liu, R. Tu, T. Goto, Construction of macroporous magnesium phosphate-based bone cement with sustained drug release, Mater. Des. 200 (2021), 109466, https://doi.org/10.1016/j.matdes.2021.109466.

[31] H. Ma, B. Xu, Y. Lu, Z. Li, Modeling magnesia-phosphate cement paste at the micro-scale, Mater. Lett. 125 (2014) 15–18, https://doi.org/10.1016/j.matlet.2014.03.143.

[32] B. Kanter, M. Geffers, A. Ignatius, U. Gbureck, Control of in vivo mineral bone cement degradation, Acta Biomater. 10 (2014) 3279–3287, https://doi.org/10.1016/j.actbio.2014.04.020.

[33] X. Liu, P. Feng, X. Shu X, Q. Ran, Effects of highly dispersed nano-SiO_2 on the microstructure development of cement pastes, Mater. Struct. 53 (2020) 1–12, https://doi.org/10.1617/s11527-019-1431-0.

[34] G. Ke, J. Zhang, Y. Liu, S. Xie, Pore characteristics of calcium sulfoaluminate cement paste with impact of supplementary cementitious materials and water to binder ratio, Powder Technol. 387 (2021) 146–155, https://doi.org/10.1016/j.powtec.2021.04.027.

[35] B. Xu, F. Winnefeld, J. Kaufmann, B. Lothenbach, Influence of magnesium-to-phosphate ratio and water-to-cement ratio on hydration and properties of magnesium potassium phosphate cements, Cement Concr. Res. 123 (2019), 105781, https://doi.org/10.1016/j.cemconres.2019.105781.

[36] I. Ali, P.A. Schneider, Crystallization of struvite from metastable region with different types of seed crystal, J. Non-Equilib. Thermodyn. 30 (2005) 95–111, https://doi.org/10.1515/JNETDY.2005.007.

[37] H. Lahalle, C. Coumes, C. Mercier, D. Lambertin, C. Cannes, S. Delpech, S. Gauffinet, Influence of the w/c ratio on the hydration process of a magnesium phosphate cement and on its retardation by boric acid, Cement Concr. Res. 109 (2018) 159–174, https://doi.org/10.1016/j.cemconres.2018.04.010.

[38] B. Xu, B. Lothenbach, A. Leemann, F. Winnefeld, Reaction mechanism of magnesium potassium phosphate cement with high magnesium-to-phosphate ratio, Cement Concr. Res. 108 (2018) 140–151, https://doi.org/10.1016/j.cemconres.2018.03.013.

[39] M. Le Rouzic, T. Chaussadent, G. Platret, L. Stefan, Mechanisms of k-struvite formation in magnesium phosphate cements, Cement Concr. Res. 91 (2017) 117–122, https://doi.org/10.1016/j.cemconres.2016.11.008.

[40] E. Soudée, J. Péra, Mechanism of setting reaction in magnesia-phosphate cements, Cement Concr. Res. 30 (2000) 315–321, https://doi.org/10.1016/S0008-8846(99)00254-9.

[41] A.S. Wagh, Chemically Bonded Phosphate Ceramics: Twenty-First Century Materials with Diverse Applications, Elsevier, 2016, https://doi.org/10.1016/C2014-0-02562-2.

[42] J. Zhang, X. Ma, D. Lin, H. Shi, Y. Yuan, W. Tang, H. Zhou, H. Guo, J. Qian, C. Liu, Magnesium modification of a calcium phosphate cement alters bone marrow

stromal cell behavior via an integrin-mediated mechanism, Biomaterials 53 (2015) 251–264, https://doi.org/10.1016/j.biomaterials.2015.02.097.

[43] A. Lode, C. Heiss, G. Knapp, J. Thomas, B. Nies, M. Gelinsky, M. Schumacher, Strontium-modified premixed calcium phosphate cements for the therapy of osteoporotic bone defects, Acta Biomater. 65 (2018) 475–485, https://doi.org/10.1016/j.actbio.2017.10.036.

[44] E. Jacobs, K. Saralidze, A.K. Roth, J.J. de Jong, J.P. van den Bergh, A. Lataster, B. T. Brans, M.L. Knetsch, I. Djordjevic, P.C. Willems, L.H. Koole, Synthesis and characterization of a new vertebroplasty cement based on gold-containing PMMA microspheres, Biomaterials 82 (2016) 60–70, https://doi.org/10.1016/j.biomaterials.2015.12.024.